Enantiomorph ‘conversion’ in the single crystals of Weyl semimetal CoSi

Wilder Carrillo-Cabrera, Paul Simon, Marcus Schmidt, Markus König, Horst Borrmann, Aimo Winkelmann, Ulrich Burkhardt, and Yuri Grin

Supporting Information

S1. Relationship between CoSi and NaCl structures

In order to understand better the "puckering" of the (010) atomic layers in CoSi, it is worthy to compare the atomic layers in the cubic structure of CoSi (A- and B form) with the equi-atomic NaCl-type layers (Figure S1). It is clear that the A- and B-form layers with unequal Co-Si distances represent very strongly distorted NaCl type layers. Due to the distortion, the coordination numbers (CN) of the atoms increase from 6 (NaCl) to 7 (CoSi).

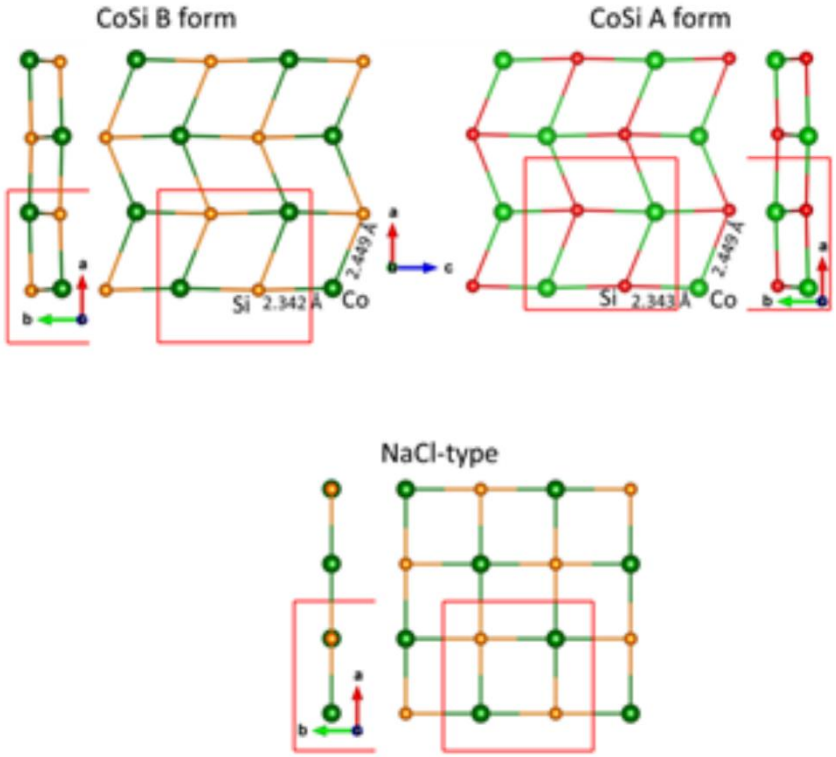

Figure S1. Comparison between the plan view and side-on views of (010) equi-atomic puckered layers in B form (y/b ≈ 0.75; and the A- form (y/b ≈ 0.75) of CoSi, (top) and hypothetical NaCl-type CoSi (bottom). The hypothetical crystal structure with the NaCl like atomic arrangement of Co and Si atoms is described by x(Co) = 0.25 and x(Si) = 0.75 for the respective Wyckoff position 4a (x, x, x). These values deviate significantly from the positions coordinates of the CoSi crystal structure (A- form: x(Co) = 0.14 and x(Si) = 0.84).

S2. Enantiomorph assignment for CoSi from complete crystal structure determination.

Table S2. Crystallographic information for the CoSi crystals 1, 2 and 3.

	Crystal 1 (A form)	Crystal 2 (B form)	Crystal 3 (A+B)
Composition	CoSi		
Space group	$P2_13$		
Pearson symbol	*cP*8		
Lattice parameter *a*, Å	4.4481(4)	4.4483(4)	4.4457(4)
Number of reflections for lattice parameter refinement	1035	1004	1009
Number of reflections measured	1120	1004	1009
$2\theta_{max}$; $\max(\sin\theta\times\lambda^{-1})$	73.27°; 0.841	73.27°; 0.841	73.27°; 0.841
Number of reflections unique	153	154	149
Measured range	$-4 \le h \le 5$ $-7 \le k \le 7$ $-7 \le l \le 7$	$-7 \le h \le 7$ $-5 \le k \le 7$ $-7 \le l \le 6$	$-6 \le h \le 6$ $-7 \le k \le 7$ $-7 \le l \le 7$
R_{int}	0.040	0.044	0.033
Number of reflections with $\lvert F \rvert > 4\sigma F$	152	154	148
Number of refined parameters	8	8	8
Flack parameter**	0.001 (1.073)	0.065 (1.053)	0.345 (0.654)
Goodness-of-fit	1.04 (1.04)	1.04 (1.04)	1.04 (1.04)
R_F; wR_{F2}	0.0144; 0.0155 (0.0311; 0.0336)	0.0176; 0.0186 (0.0322; 0.0347)	0.0158; 0.0167 (0.0206; 0.0221)
x for Co in 4(*a*) *xxx*	0.14348(6) (0.8565(2))	0.85648(7) (0.1436(2))	0.14345(7) (0.85652(9))
x for Si in 4(*a*) *xxx*	0.8439(2) (0.1561(3))	0.1562(2) (0.8338(3))	0.8437(2) (0.1563(2))
ADP_{Co}: U_{11}; U_{12}*	0.0055(2); 0.00027(8) (0.0055(3); 0.0003(2))	0.0059(2); 0.00031(9) (0.0058(4); 0.0003(2))	0.0053(2); 0.00024(8) (0.0052(3); 0.0002(1))
ADP_{Si}: U_{11}, U_{12}*	0.0056(2) -0.0003(2) (0.0057(4); -0.0002(4))	0.0057(2); -0.0004(2) (0.0058(4); -0.0004(4))	0.0055(2); -0.0004(2) (0.0055(3); -0.0004(3))

*Symmetry constrains $U_{22} = U_{33} = U_{11}$; $U_{13} = U_{23} = U_{12}$.

** For crystals 1 and 3: refined as A (refined as B); for crystal 2: refined as B (refined as A).

S3. Enantiomorph assignment for CoSi from EBSD analysis.

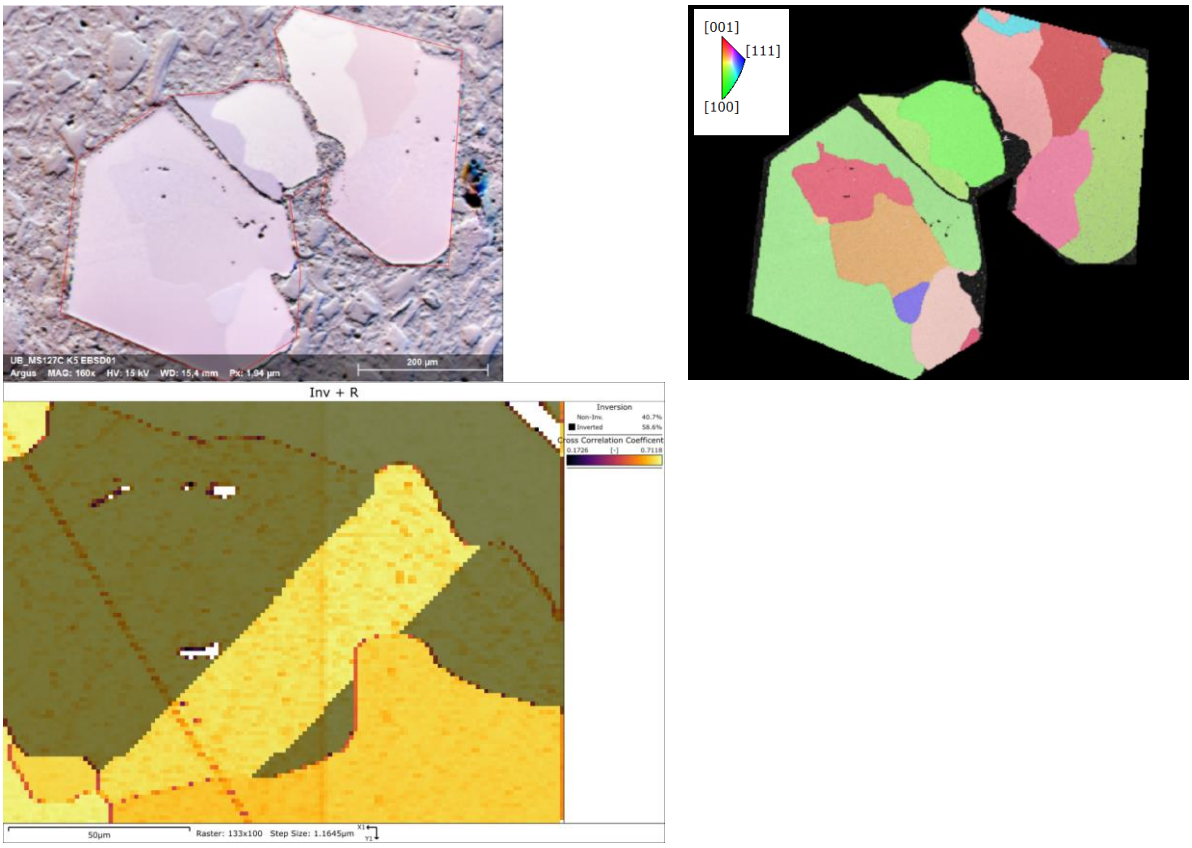

Figure S3 (top left): Microstructure of the mCVT-prepared CoSi crystallite 2 of Figure 1 (top left) recorded with the fore-scattered electron detector. (top right): Inverse pole figure z (IPFZ) of crystallite 2. The left, red coloured grain with [001] direction oriented perpendicular to the cross-section plane are used for TEM preparation (inset): colour code of the unit cell direction perpendicular to the sample surface. (bottom) enantiomorph distribution map of the areas close to the grain with [001] orientation. Areas assigned to the A- form and B- form are shown in bright or dark, respectively.

S4. Transmission electron microscopy

All selected areas for FIB sectioning were positioned perpendicular to a (010) twin boundary. For the FIB lamellae fabrication, first, the selected areas (top black lines on yellow dashed rectangles in Fig.1) were covered with protective platinum layers (2 µm thickness), applying an acceleration voltage of 30 kV and a current of 0.1 nA. Second, the oriented 2 µm thick FIB cross-sections were cut by the lift-out technique [1] and after being transferred to molybdenum half-rings were further thinned down to electron transparency to a thickness of about 40 mm, using an acceleration voltage of 30 kV and currents of 3–0.1 nA. In the final stage, the FIB cuts were polished to a thickness of about 20 nm by applying a low acceleration voltage of 5 kV and a current of 0.3 nA.

It should be mentioned that the defined crystallographic alignment of the oriented FIB cuts could be successfully realized because of the previous knowledge of the absolute crystal orientation determined by the EBSD method [2]. Also, because the required cross-sections were inclined to the sample surface, after protecting Pt layer covering the polished sample was rotated to different angles before FIB cross-section manufacturing (to about –35° for [101] cut and to about 55° for $[10\bar{1}]$ cut). For the most inclined $[00\bar{1}]$ FIB case, a nearly cubic fragment (~20×20×20 µm, marked by a white rectangle in Fig. 1) was manufactured in several stages, first extracted, rotated 90°, transferred to a molybdenum half-ring, Pt layer covered, further rotated about 10°, manufactured to a 2 µm thin FIB cut, and moved to another molybdenum half-ring for final thinning.

In the preliminary TEM study on long FIB lamellae (12 to 20 µm), there were some difficulties to find the enantiomorph exchange area (it should be visible as a line in the perpendicular cross-sections). Contrast aperture, defocusing and tilting (~10°) are necessary to make the twin interface observable at low magnifications. By the HR-TEM imaging at high magnifications to find the twin interface it was very difficult, even more for the HR-STEM imaging.

For large magnifications in the HR-STEM microscope, it is very difficult to find the twin interface, but we use different prominent topographic marks (created during FIB thinning at the top of the FIB lamella) to localized more or less the interface, then after orienting the lamella perpendicular to [010] direction, we use the effective difference in height [e.g. $(a/2 - t)$ or $(a - 2t)/(2\sqrt{2})$] of the prominent structure features to localize the enantiomorph exchange area.

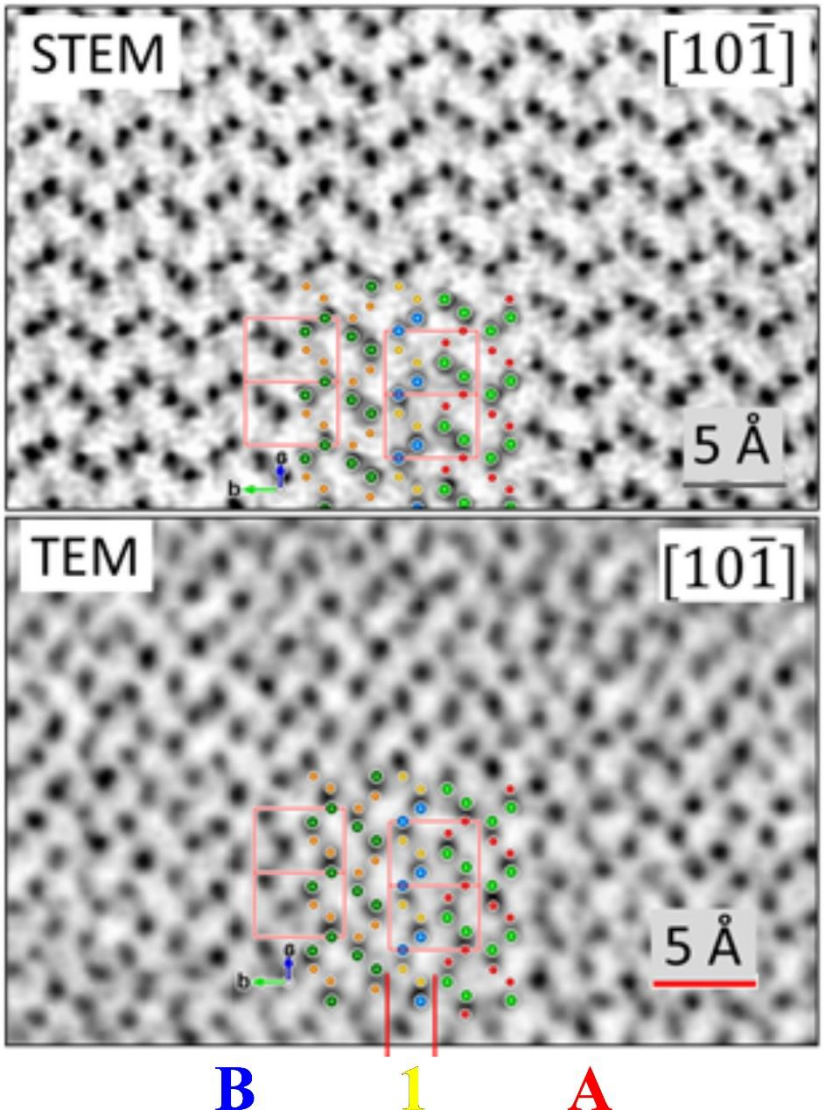

Figure S4. Comparison of aberration-corrected HAADF STEM (top) and HR-TEM (bottom) images of enantiomorph exchange area as viewed along [10$\bar{1}$] direction (the original dark grey colour of the images was inverted). The enantiomorph exchange area is observed in the middle of the figures (blue Co atoms). Corresponding projections of the structure model are superposed on the images (red, orange: Si, light, dark green Co). In STEM the Co atom columns are well resolved (Si columns are weak), but in TEM the Co-Si dumbbells are not resolved (ca 0.96 Å distance) and both together appear as one spot.

S5. Structure model for the atomic decoration of the enantiomorph exchange region

The crystal structure of the CoSi phase shows the symmetry of the space group $P2_13$ and the periodicity a = 4.4484 Å. The crystal structure is chiral and both enantiomorphs – A- and B- form - show the symmetry of the same space group. The Co and Si atoms occupy Wyckoff sites 4*a* (*x x x*) with *x*(Co) = 0.1435, *x*(Si) = 0.8439 for the A- form and *x*(Co) = 0.8565, *x*(Si) = 0.1562 for the B- form (Table S2).

Within the cubic unit cell, two atoms of each element show for each of the coordinates x, y, z values ≅ ¼ and ≅ ¾. Thus, these groups of 4 atoms form two layers around ¼ and ¾ perpendicular to the cubic main axes {100}. These are not layers in the sense of chemical bonding or chemically stable structure fragments. Interatomic inter-layer distances are very close to the intra-layer distances. So, these layers represent a formal grouping of atoms due to their coordinates. These arguments hold for all three main axes of the cubic unit cell of the CoSi crystal structure. In the present description, we choose the layers perpendicular to the [010] direction because of our experimental results. The layer formed by the atoms at $y \cong ¼$ of the A form, we denote by $(010)_A{}^{¼}$, the term $(010)_A{}^{¾}$ describes the atoms at $y \cong ¾$. The two layers are related by the 2_1 screw axes (Table S5-1). So, the layers show the same atomic arrangement but rotated by 180° in respect to the position of the 2_1 screw axis. Alternatively, the atomic arrangements of the layer $(010)_A{}^{¼}$ and $(010)_A{}^{¾}$ are related by a shift $\vec{v}$ = (*x*(Si) – *x*(Co) – ½) $\vec{a}$ + ½ $\vec{b}$ combined with the exchange of the elements. The deviations along $\vec{b}$ and $\vec{c}$ amount ±|1- (*x*(Si) + *x*(Co)|, while change of the *x* coordinates is the same for all positions (Table S5-2). It should be noticed that the two transformations– e.g. the 2_1 screw axis and shift plus element exchange – which transforms the atomic positions of $(010)_A{}^{¼} \rightarrow (010)_A{}^{¾}$ results exactly the same atomic arrangement if *x*(Si) + *x*(Co) = 1.

For the understanding of the crystal structure, it is important to note that the two enantiomorph variants differ essentially by the exchange of the two elements on all atomic positions. For an idealized crystal structure with *x*(Co) + *x*(Si) = 1, the coordinates of the atomic positions are identical and Co atoms occupy the Si positions and vice versa. Consequently, the exchange of the elements on the positions of layer $(010)_A{}^{¼}$ results an atomic arrangement which is almost identical with the layer $(010)_B{}^{¼}$ as well as with the layer $(010)_A{}^{¾}$. Also holds, that the atomic arrangements of the layers $(010)_A{}^{¾}$ and $(010)_B{}^{¼}$ are almost identical (Table S5-3). These pairs of layers are identical for an idealized structure with *x*(Co) + *x*(Si) = 1

An initial model which describes the atom arrangement in the transition region is derived essentially from one common atomic layer which connects the two half crystals with opposite handedness. Starting from the common layer $(010)_A{}^{¾}$ in the middle of the transition region of the HR-TEM image (Figure 4) means the sequence of the layers of the A form …$(010)_A{}^{¾}(010)_A{}^{¼}(010)_A{}^{¾}$ $(010)_A{}^{¼}(010)_A{}^{¾}$…describe the atomic arrangements of the right half crystal. The same common starting layer can be notated by $(010)_B{}^{¼}$ and the sequence of the layers of the B form …$(010)_B{}^{¼}(010)_B{}^{¾}(010)_B{}^{¼}(010)_B{}^{¾}(010)_B{}^{¼}$… describe the atomic arrangements of left half crystal. The pattern of the three HR-STEM images along different zone axes are described by this model consistently. This means that the investigated transition region does not show additional twinning or translation components parallel to one of the chosen zone axes. Also, it should be noticed that the EBSD-based assignment of the handedness is essential for this interpretation of the HR-STEM images. Without the knowledge of the handedness, the pattern of the atom columns allows to interpret the common layer as $(010)_A{}^{¼}$ (respective $(010)_B{}^{¾}$) and also to assign the A form to the pattern of the left half crystal and the B form to the pattern of the right half crystal.

The observed atomic arrangement of the transition region, which connects the two domains of opposite handedness, can thus be described as a stacking variant of almost un-altered atomic layers of the CoSi structure. This is a remarkable result because it tracebacks the change of the handedness of the real structure of CoSi to a two-dimensional stacking fault. A detailed graphical representation of the layer sequence at the transition region is shown in Figure S5-1.

Due to the change in the stacking sequence of the layers, the change in handedness is associated with atomic arrangements that do not occur in the crystal structure of CoSi. For their detailed consideration, quantum chemical calculations were carried out on the basis of an atomic model describing the transition region. The initial configuration for this model contains the 8 atomic positions of two adjacent unit cells of the A form, which are linked by an inversion centre to corresponding positions of the B form. The inversion centre is located in the plane $(010)_A{}^{¾}$. The pairs of atomic positions of the planes $(010)_A{}^{¾}$ and

$(010)_B$¼ which are closely spaced by the inversion mapping, are represented by one, averaged position each, so that a transition plane $(010)_I$ is formed. The inversion centre is situated at (0.6 ¾ 0)$_A$ or (0.4 ¼ 0)$_B$ of the A-form or B-form unit cell. The described structural fragment is bounded by two additional planes $(010)_I$, whose inversion centre also causes the change of handedness. This structure model for the enantiomorph exchange region comprises thus four unit cells of CoSi size and has the symmetry of the space group $P2_1/c$ and periodicities described by the lattice parameters $a_{mon} = b_{mon} = a_{cub} = 4.447$ Å, $c_{mon} = 4 \times a_{cub} = 17.788$ Å whereby the monoclinic angle is $\beta = 90°$. Presence of a higher symmetry was excluded analysing by the software Platon [3]. The shortest interatomic distances of CoSi and the $P2_1/c$ structure model are compared in Tables S5-4 and S5-5. The change of handedness occurs after a distance of $2 \times a_{cub}$ (= ½ c_{mon}, Figure S5-2). Within the monoclinic unit cell, the observed atomic arrangements at the transition region are well described by the $P2_1/c$ model. A graphical representation of the structure model in Figure S5-2 visualize the relations between the cubic unit cells of the A and B form and the monoclinic unit cells with inversion centres. The basis for the quantum chemical calculation is the energy-optimized structure model (Table S5-6). Up to our best knowledge this crystal structure is not realized in any binary system.

Table S5-1. Coordinates of symmetry-related Co and Si atoms in the A form of CoSi.

Space group $P2_13$; a = 4.4481 Å; Wyckoff site 4a (x x x) with x_{Co} = 0.1435; x_{Si} = 0.8439.

	Atom	x	y	z
x, x, x	Si_1	0.8439	0.8439	0.8439
	Co_1	0.1435	0.1435	0.1435
$-x+½, -x, x+½$	Si_2	0.6561	0.1561	0.3439
	Co_2	0.3565	0.8565	0.6435
$-x, x+½, -x+½$	Si_3	0.1561	0.3439	0.6561
	Co_3	0.8565	0.6435	0.3565
$x+½, -x+½, -x$	Si_4	0.3439	0.6561	0.1561
	Co_4	0.6435	0.3565	0.8565

Table S5-2: Comparison of the atomic positions in layer $(010)_A^{¼}$ and their related position in layer $(010)_A^{¾}$. The layers $(010)_A^{¼}$ and $(010)_A^{¾}$ are related by the shift $\vec{v}$ = 0.2 $\vec{a}$ + ½ $\vec{b}$ combined with the interchange of the elements Co and Si.

$(010)_A^{¼}$	$(010)_A^{¾}$	Δ_x	Δ_y - 0.5	Δ_z
Si_4	Co_3	0.2004	-0.0126	+0.0126
Si_2	Co_2	0.2004	+0.0126	-0.0126
Co_1	Si_4	0.2004	+0.0126	+0.0126
Co_2	Si_1	0.2004	-0.0126	-0.0126

Table S5-3. Comparison of the atomic positions in layer $(010)_A^{¾}$ and their related positions in layer $(010)_B^{¼}$. The coordinates of $(010)_B^{¼}$ are calculated from the coordinates of the atoms of layer $(010)_A^{¼}$ by inversion plus shift along ($\vec{a}$ + $\vec{b}$ + $\vec{c}$) + $\vec{v}$.

$(010)_A^{¾}$	$(010)_B^{¼}$	Δ_x	Δ_y	Δ_z
Co_3	Co_3	-0.0126	0	0
Co_2	Co_2	-0.0126	0	0
Si_4	Si_4	+0.0126	0	0
Si_1	Si_1	+0.0126	0	0

Table S5-4:

Shortest interatomic distances of the CoSi crystal structure with cubic symmetry (space group $P2_13$; lattice parameter a_{cub} = 4.4481 Å)

Co – Si	2.311 Å	Co - Co	2.735 Å (6x)	Si – Si	2.754 (6x)
	2.343 Å (6x)		3.990 Å (6x)		3.872 (6x)
	2.451 Å (6x)				

Table S5-5:

Shortest interatomic distances of the hypothetical structure model with monoclinic symmetry (space group $P2_1/c$; lattice parameter $a_{mon} = b_{mon} = a_{cub} = 4.4481$ Å, $c_{mon} = 4 \times a_{cub} = 17.792$ Å; $\beta = 90°$

Co – Si	2.262 Å (Co4-Si2)	Co - Co	2.714 Å Co2-Co4	Si – Si	2.723 Å (Si2-Si4) (Si2-Si3)
	2.311 Å (Co3-Si1) (Co1 – Si3)		2.7333 Å (Co1-Co4) (Co3-Co4)		2.752 Å (Si1-Si4)
	2.358 Å (Co2-Si3)				

Table S5-6. Atomic coordinates for a hypothetical monoclinic CoSi model. Space group $P2_1/c$, No. 14; a = 4.4481 Å, b = 4.4481 Å, c = 17.792 Å, β = 90°.

Atom	Site	*x*	*y*	*z*
Co1	4*e*	0.14353	0.25642	0.27663
Co2	4*e*	0.14997	0.24998	0.02499
Co3	4*e*	0.35647	0.54347	0.15160
Co4	4*e*	0.64353	0.04354	0.09839
Si1	4*e*	0.65641	0. 24353	0.22659
Si2	4*e*	0.35003	0.74988	0.02499
Si3	4*e*	0.15641	0.05636	0.14838
Si4	4e	0.15641	0.05636	0.39839

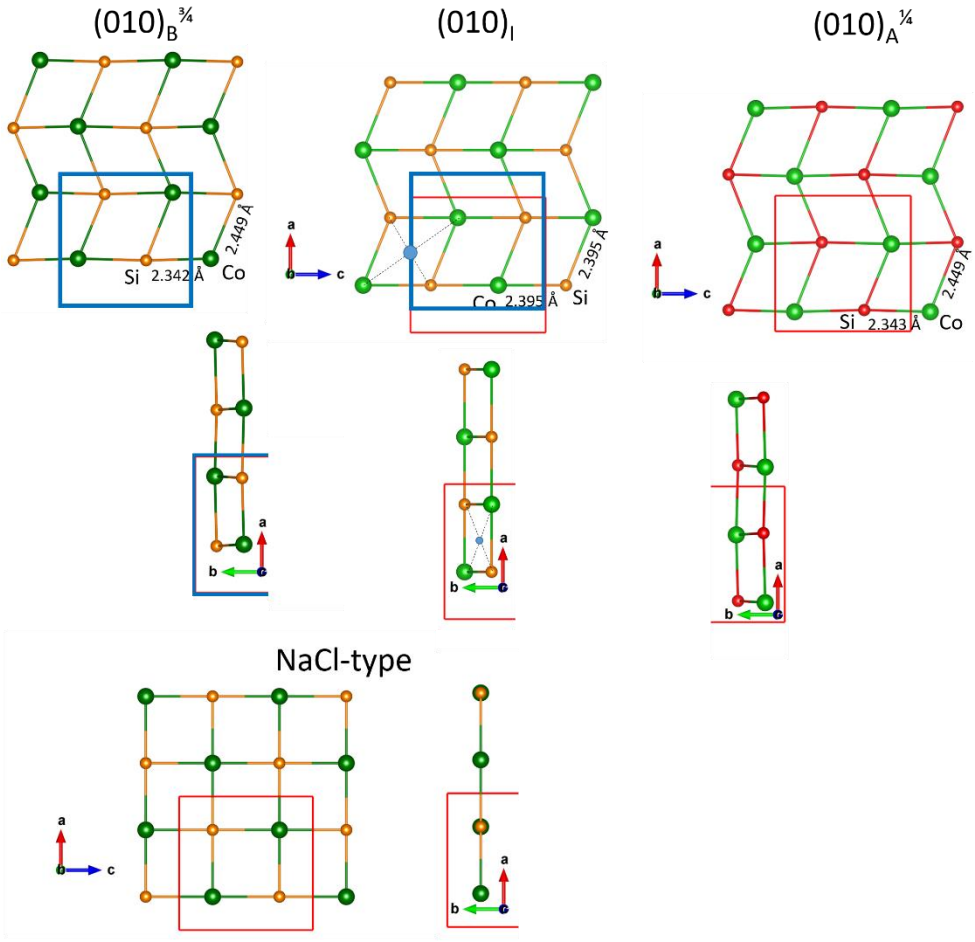

Figure S5-1: Comparison between the plan view and side-on views of (010) layers at the transition region: (top) Layer sequence along the [0$\bar{1}$0] direction: $(010)_B{}^{3/4}(010)_I(010)_A{}^{¼}$, the inversion centre (blue circle) is situated at the interface layer $(010)_I$ (middle) side view of the layer sequence. (bottom) Hypothetical NaCl-type CoSi, CN(Co) = 6, with *x*(Co) = 0.25, *x*(Si) = 0.75 e.g. *x*(Co) + *x*(Si) = 1; *x*(Si) – *x*(Co) = 0.5 representing a centrosymmetric atomic arrangement.

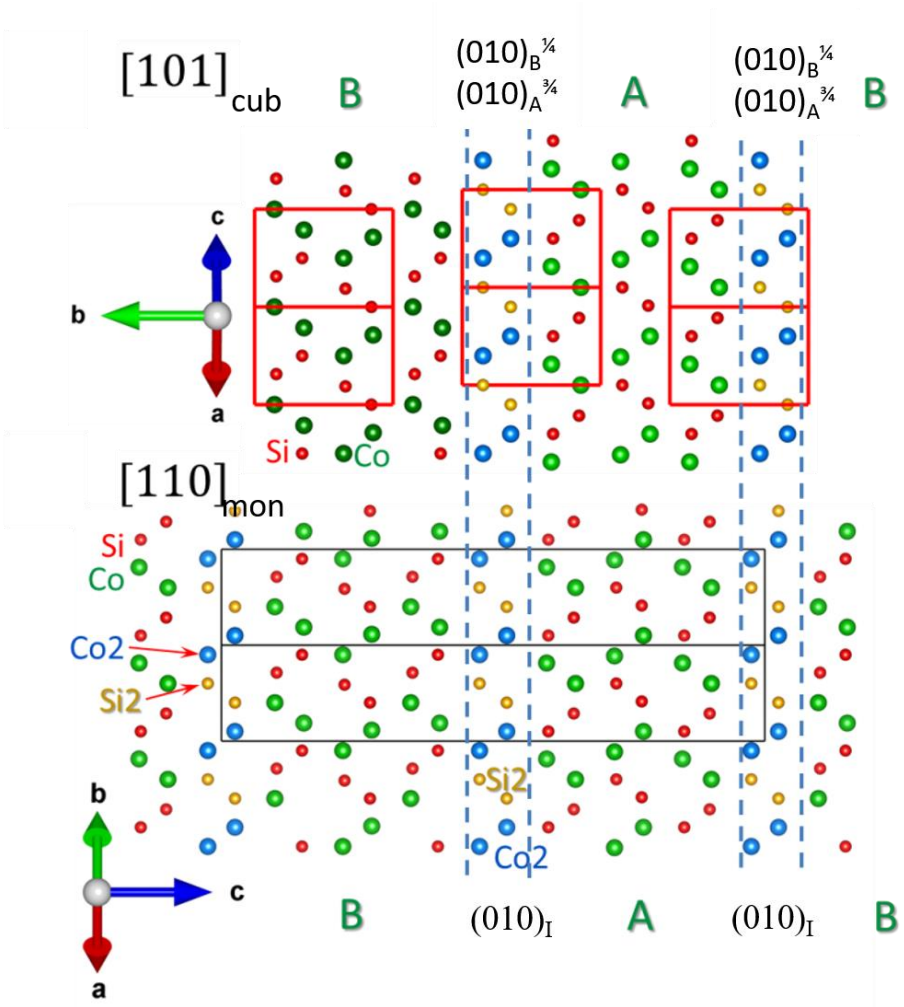

Figure S5-2. Relation between the cubic unit cells of the A- and B- form of CoSi and the monoclinic unit cell of the hypothetical, periodic structure model. (top) projection along [101] of the cubic unit cell (red) of CoSi. The fragments with opposite handedness are linked by $(010)_I$ layers (dashed blue lines) which is strongly related to the layers $(010)_A^{¾}$ and $(010)_B^{¼}$ of the pristine CoSi crystal structure of the A- and B- form. The hypothetical inversion center is located at (0.6, ¾, 0)$_A$ or (0.4, ¼, 0)$_B$. (bottom) the same projection of the structure model with monoclinic unit cell (black straight lines). The inversion centers are situated at (0, 0, 0) and (0, 0, ½).

S6. Chemical bonding in CoSi

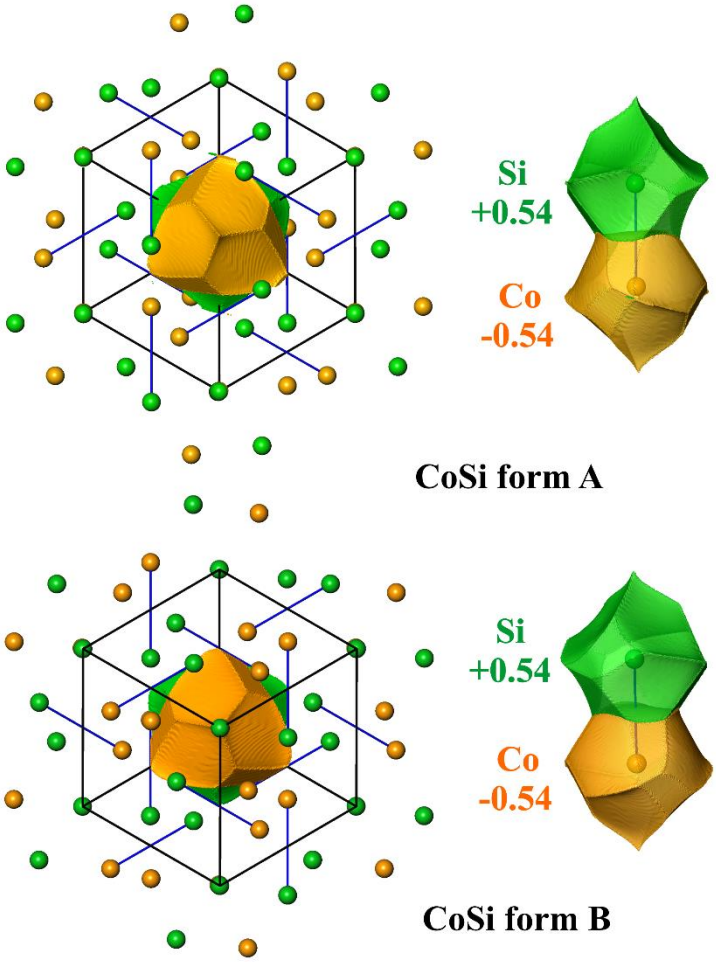

Figure S6-1. QTAIM atomic basins and effective charges in enantiomorphs of CoSi.

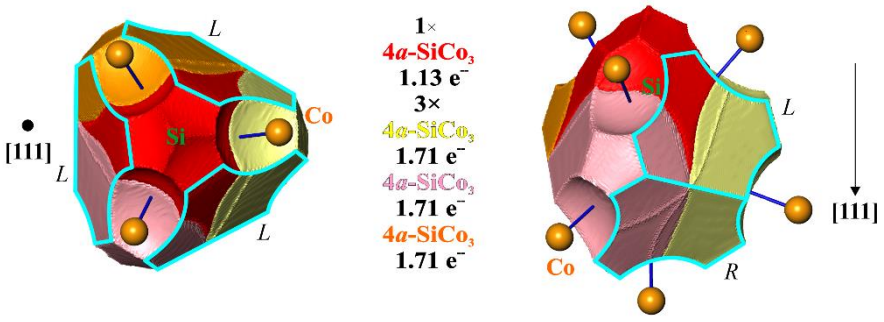

CoSi form B

Figure S6-2. ELI-D bond basins in Co-Si unit in form B of CoSi.

References

[1] I. Antonyshyn, F. R. Wagner, M. Bobnar, O. Sichevych, U. Burkhardt, M. Schmidt, M. König, K. Poeppelmeier, A. P. Mackenzie, E. Svanidze, Y. Grin. Angew. Chem. Int. Ed. 2020, 59, 11136-11141.

[2] U. Burkhardt, H. Borrmann, P. Moll, M. Schmidt, Yu. Grin, A. Winkelmann. Scientific Reports 10 (2020) 4065.

[3] A. L. Spek. J. Appl.Crystallogr. 36, 2003, 7-11.